Projections of Quantum Observables onto Classical Degrees of Freedom in Mixed Quantum-Classical Simulations: Understanding Linear Response Failure for the Photoexcited Hydrated Electron

Michael J. Bedard-Hearn, Ross E. Larsen, and Benjamin J. Schwartz*

Department of Chemistry and Biochemistry, UCLA, 607 Charles E. Young Drive East, Los Angeles, California 90095-1569, USA
(Received 10 April 2006; published 27 September 2006)

We present a general analytic method for understanding how specific motions of a classical bath influence the dynamics of quantum-mechanical observables in mixed quantum-classical molecular dynamics simulations. We apply our method and develop expressions for the special case of quantum solvation, allowing us to examine how specific classical solvent motions couple to the equilibrium energy fluctuations and nonequilibrium energy relaxation of a quantum-mechanical solute. As a first application of our formalism, we investigate the motions of classical water underlying the equilibrium and nonequilibrium excited-state solvent response functions of the hydrated electron; the results allow us to explain why the linear response approximation fails for this system.

One of the principal goals of molecular dynamics (MD) simulations is to understand how specific molecular motions of a bath influence physical processes of interest. Often, the dynamics are analyzed using the linear response (LR) approximation, which assumes that the solvent motions that respond to a perturbation are the same as the motions that cause fluctuations at equilibrium. When LR holds, equilibrium MD can be used to understand the molecular origins of relaxation. For instance, when LR applies, one can use the Steele theory [1,2] to project exactly how a dynamical variable is changed by specific bath degrees of freedom. Ladanyi and co-workers have assumed LR and employed such projections with equilibrium MD to understand how specific bath motions affect classical solvation dynamics [2,3]. Recently, we extended the classical projections formalism to nonequilibrium MD, and uncovered a hidden breakdown of LR [4]. Despite their successful use in classical simulations, however, there has been no analogous projection technique for understanding how bath degrees of freedom (DOF) affect quantum-mechanical observables. In this Letter, we present a new formalism for projecting dynamical changes of quantum expectation values in mixed quantum-classical (MQC) simulations onto classical molecular motions. Our method allows us to determine how any measurable quantity associated with a quantum wave function is affected by specific motions of a classical bath.

In classical MD, projections are performed by expanding the time derivative of an observable A using the chain rule, $\dot{A} = \sum_i \dot{\mathbf{R}}_i \cdot \boldsymbol{\nabla}_{\mathbf{R}_i} A$, where $\mathbf{R}$ denotes the bath coordinates and the index i runs over all bath DOF. Integration of each term in the sum with respect to time gives A_i, the projection of A onto bath coordinate i [4,5]. Here, we use a similar approach to project quantum expectation values onto bath coordinates, and after presenting our new formalism, we apply it to one of the best-studied MQC systems,

the hydrated electron [6]. Our analysis shows clearly why LR fails to describe the nonequilibrium solvent relaxation following photoexcitation of this prototypical quantum solute.

In MQC simulations, the Hamiltonian of the quantum subsystem is $\hat{H} = \hat{T} + \hat{U}$, where $\hat{T}$ and $\hat{U}$ are the quantum-mechanical kinetic and potential energy operators and $\hat{U}$ depends on both the classical ($\mathbf{R}$) and quantal DOF. For a given configuration of the classical particles, the quantum subsystem is defined in terms of the adiabatic eigenvectors ($|k\rangle$) and eigenvalues (E_k) of $\hat{H}$, and evolves according to the classical dynamics and the time-dependent Schrödinger equation (TDSE). The classical subsystem's dynamics are, in turn, driven by both the classical interaction potential and the Hellmann-Feynman (HF) force, $\mathbf{F}^i = -\langle\psi|\boldsymbol{\nabla}_{\mathbf{R}_i}\hat{U}|\psi\rangle$, which is the force the quantum subsystem with wave function $|\psi\rangle$ exerts on each classical DOF, $\mathbf{R}_i$. Although the above prescription dictates the precise evolution of a MQC system, it does not provide information as to which *specific* classical DOF influence the dynamics of any quantum observable.

To obtain such information, our goal is to emulate the classical Steele theory and write the time derivative of a quantum expectation value in terms of classical gradients. Consider a quantum Hermitian operator $\hat{\Omega}$ and its expectation value with the kth adiabatic state, $\langle k|\hat{\Omega}|k\rangle \equiv \Omega_{kk}$. Using the chain rule,

$$\frac{d}{dt}\langle k|\hat{\Omega}|k\rangle = \langle \dot{k}|\hat{\Omega}|k\rangle + \langle k|\hat{\Omega}|\dot{k}\rangle + \langle k|\dot{\hat{\Omega}}|k\rangle, \quad (1)$$

inserting a complete set of states into the first two terms on the right-hand side of Eq. (1), and introducing the non-adiabatic coupling vectors, $\langle m|\dot{k}\rangle = \sum_i \dot{\mathbf{R}}_i \cdot \langle m|\boldsymbol{\nabla}_{\mathbf{R}_i}k\rangle \equiv \sum_i \dot{\mathbf{R}}_i \cdot \mathbf{d}^i_{mk}$, we obtain

$$\dot{\Omega}_{kk} = \sum_i \left[2\sum_m \dot{\mathbf{R}}_i \cdot \mathbf{d}^i_{km}\Omega_{mk} + \dot{\mathbf{R}}_i \cdot \langle k|(\boldsymbol{\nabla}_{\mathbf{R}_i}\hat{\Omega})|k\rangle \right]$$

$$\equiv \sum_i \dot{\Omega}^i_{kk}, \qquad (2)$$

where m and k index the adiabatic eigenstates of $\hat{H}$, $\Omega_{mk} \equiv \langle m|\hat{\Omega}|k\rangle$, and the sum on i runs over the classical DOF. Although the sum on m formally runs over all states, it likely can be truncated in many practical applications. Thus, Eq. (3) shows that projections of Ω_{kk} onto specific classical coordinates depend on how the velocities of relevant classical DOF alter the adiabatic eigenstates, which in turn alter the quantum expectation value.

Equation (2) is valid for expectation values associated with a single adiabatic state, but in nonadiabatic MQC simulations, the quantum subsystem is often described as a superposition of adiabatic eigenvectors, $|\psi\rangle = \sum_k a_k|k\rangle$, or a mean-field (MF) state. The projections for quantum observables associated with MF states proceed in a similar manner as for adiabatic states, but the evolution of the density matrix, $\rho_{kk'} = a^*_k a_{k'}$, leads to an unusual cancellation of terms. Using the TDSE,

$$\dot{\rho}_{kk'} = \sum_{m,i} \dot{\mathbf{R}}_i \cdot (\rho_{mk'}\mathbf{d}^i_{mk} - \rho_{km}\mathbf{d}^i_{k'm}) + \frac{i}{\hbar}\rho_{kk'}E_{kk'}, \quad (3)$$

where $E_{kk'} = E_k - E_{k'}$, we see that

$$\frac{d}{dt}\langle\psi|\hat{\Omega}|\psi\rangle = \frac{i}{\hbar}\sum_{k,k'}\rho_{kk'}\Omega_{kk'}E_{kk'} + \sum_i \dot{\mathbf{R}}_i \cdot \langle\psi|\boldsymbol{\nabla}_{\mathbf{R}_i}\hat{\Omega}|\psi\rangle$$

$$\equiv \frac{i}{\hbar}\sum_{k,k'}\rho_{kk'}\Omega_{kk'}E_{kk'} + \sum_i \dot{\Omega}^i, \qquad (4)$$

where the nonadiabatic coupling terms from the derivatives of the eigenvectors [cf. Eq. (2)] exactly cancel the identical terms from the derivative of the density matrix in Eq. (3). The first term in the final expression of Eq. (4) arises from quantum phase evolution in the TDSE; it has no explicit dependence on the classical particles' motions and vanishes if either $\hat{\Omega}$ or the density matrix is diagonal in the chosen basis. In addition, if $\hat{\Omega}$ has no explicit $\mathbf{R}$ dependence, then the second term in the final expression of Eq. (4) also vanishes, so there appears to be no expression analogous to Eq. (2) that determines how the bath DOF influence expectation values associated with quantum superposition states. If $\hat{\Omega}$ does have explicit $\mathbf{R}$ dependence, however, then the second term in Eq. (4) provides the desired information. For either Eq. (2) or Eq. (4), the projection onto a classical coordinate i is found by integrating either $\dot{\Omega}^i_{kk}$ or $\dot{\Omega}^i$ with respect to time,

$$\Omega^i(t) - \Omega^i(0) = \int_0^t dt' \dot{\Omega}^i(t'). \qquad (5)$$

Thus, Eqs. (2), (4), and (5) allow us to project the dynamics of quantum solutes, even those described by superposition wave functions, onto specific motions of a classical bath.

To illustrate the application of our formalism in MQC simulations, we consider the case of a classical solvent causing the energy of a quantum solute to relax following excitation. The nonequilibrium relaxation dynamics are described by the solvent response function,

$$S(t) = [\overline{\Delta E}(t) - \overline{\Delta E}(\infty)]/[\overline{\Delta E}(0) - \overline{\Delta E}(\infty)], \quad (6)$$

where the overbar denotes a nonequilibrium ensemble average and $\Delta E = \langle\psi|\hat{H}|\psi\rangle - \langle 0|\hat{H}|0\rangle$ is the energy gap between the excited ($|\psi\rangle$) and ground ($|0\rangle$) states of the quantum solute. In the limit of LR, the nonequilibrium response function is equal to the equilibrium solvation correlation function,

$$C(t) = \langle\delta\Delta E(t)\delta\Delta E(0)\rangle/\langle(\delta\Delta E)^2\rangle, \qquad (7)$$

where the fluctuations from the average energy gap [7] are $\delta\Delta E(t) = \Delta E(t) - \langle\Delta E\rangle$, and the angled brackets denote an equilibrium ensemble average. [Although LR implies that $S(t) \sim C(t)$, the converse is not necessarily true—the breakdown may be hidden [4].]

To project the nonequilibrium and equilibrium solvation dynamics onto the motions of classical particles, we take the first time derivative, $J(t) \equiv \dot{S}(t)$, of Eq. (6),

$$J(t) = \sum_i \overline{\Delta\dot{E}_i}(t)/(\overline{\Delta E}(0) - \overline{\Delta E}(\infty)) \equiv \sum_i J_i(t), \quad (8)$$

and the second derivative, $G(t) \equiv -\ddot{C}(t)$, of Eq. (7),

$$G(t) = \sum_{i,j} \frac{\langle\Delta\dot{E}_i(t)\Delta\dot{E}_j(0)\rangle}{\langle(\delta\Delta E)^2\rangle} \equiv \sum_{i,j} G_{ij}(t). \qquad (9)$$

By numerically integrating each projected $J_i(t)$ once and each $G_{ij}(t)$ twice with respect to time [4] and finding the appropriate constants of integration (see EPAPS supplementary material [14]), we obtain the desired nonequilibrium and equilibrium projections, $S_i(t)$ and $C_{ij}(t)$, respectively. Since both Eqs. (8) and (9) have $\hat{\Omega} = \hat{H}$, the desired derivatives from Eqs. (2) and (4) are

$$\frac{d}{dt}\langle k|\hat{H}|k\rangle = -\sum_i \dot{\mathbf{R}}_i \cdot \mathbf{F}^i_k \equiv \sum_i \dot{E}^i_k,$$

$$\frac{d}{dt}\langle\psi|\hat{H}|\psi\rangle = -\sum_i \dot{\mathbf{R}}_i \cdot \mathbf{F}^i \equiv \sum_i \dot{E}^i, \qquad (10)$$

where $\mathbf{F}^i_k = -\langle k|\boldsymbol{\nabla}_{\mathbf{R}_i}\hat{H}|k\rangle$ is the adiabatic HF force. The classical Cartesian velocities $\dot{\mathbf{R}}_i$ can be converted into relative solute-solvent coordinates via unitary transformations. For example, the center-of-mass (c.m.) velocity of each classical particle can be separated into a longitudinal translation (directly toward or away from the quantum solute's center of mass) and two lateral orthogonal translations. Equations (8)–(10) provide everything needed to quantify exactly how specific classical solvent motions such as translations or rotations affect the solvation dynamics of quantum solutes. They are analogous to the

classical projection formalism [2,4]; the difference is that the force in Eq. (10) is not classical but is instead the HF force, as appropriate for a MQC system.

We now apply these new tools [Eqs. (8) and (9)] to explore the molecular basis of solvation following photo-excitation of the hydrated electron (e_{hyd}^-). The details of our MQC simulations are given elsewhere [8]; briefly, the system contains 200 classical SPC-Flex water molecules [9] and a single excess quantum electron that interacts with the solvent via a pseudopotential [10]. To study the equilibrium solvent response [Eq. (7)] of the e_{hyd}^-, we ran two uncorrelated 50-ps trajectories in which the electron was confined to its adiabatic ground state and the velocity Verlet algorithm was used to propagate the classical dynamics with a time step of 1 fs. To study the nonequilibrium solvent relaxation [Eq. (6)], we ran 50 nonequilibrium trajectories (using a 0.125-fs time step), with initial configurations taken from 25 uncorrelated configurations extracted from the equilibrium trajectories (with initial velocities reversed to obtain a second initial condition per starting configuration). Each nonequilibrium trajectory mimicked a one-photon Frank-Condon excitation by instantly promoting the electron to an adiabatic excited state 2.27 ± 0.01 eV above the ground state and concluding when the e_{hyd}^- nonadiabatically returned to the ground state.

Previous calculations by Schwartz and Rossky [6] found that $S(t)$ is similar to $C(t)$ for the excited e_{hyd}^-, suggesting that LR holds for this system. This result is surprising given that studies of classical solvation have shown that when solutes change size or shape, LR typically does not apply [15]. Since the hydrated electron undergoes a shape change upon excitation (from s-like to p-like), we expect that the underlying dynamics coupling to the equilibrium and nonequilibrium solvation processes should be quite different. Hence, we have revisited the solvation dynamics of this system, and Fig. 1(a) shows that $S(t)$ and $C(t)$ are in fact different, even at the earliest times when the LR approximation is expected to be most applicable. The difference between our results and those in Ref. [6] may stem from the different nonadiabatic MQC algorithms used here and in Ref. [6] (see Ref. [8]), or from the poor statistical sampling in Ref. [6], which used only 20 nonequilibrium trajectories instead of the 50 used here [16].

To understand the breakdown of LR for the e_{hyd}^- evident in Fig. 1(a), we calculated time-integrated projections of both the nonequilibrium [Fig. 1(a), Eq. (8)] and equilibrium [Fig. 1(b), Eq. (9)] solvent response functions onto various classical DOF. Figure 1 shows such projections onto the water c.m. translations, S_{trans} and C_{trans}, as well as the longitudinal component of the water c.m. translations (discussed above), S_{long} and C_{long}. The figure also shows the sum of the projections onto all the rotational and vibrational DOF, taken as the difference between the total solvent response and the total c.m. translational projection,

i.e., $S_{r-v} = S_{tot} - S_{trans}$; we note that C_{r-v} also contains cross terms that do not appear in the nonequilibrium projections [2,4].

The water molecules in our simulations are flexible, so there is no strict way to project separately their vibrational and rotational motions. As a result, we separated the contributions of rotational and vibrational modes using Fourier analysis. The librational modes of SPC-Flex water have frequencies less than ~1000 cm^{-1} and are spectrally well separated from the vibrational modes, whose frequencies
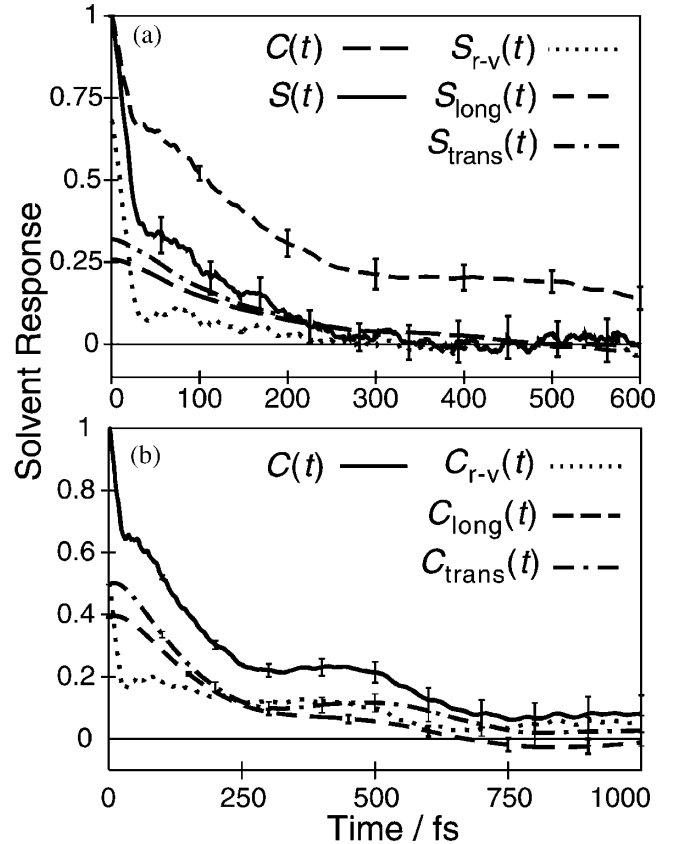

FIG. 1. (a) Comparison between the total nonequilibrium, $S(t)$, and equilibrium, $C(t)$, solvent response functions [Eqs. (6) and (7)] showing the breakdown of LR for the e_{hyd}^-. Integrated projections of the nonequilibrium solvent response onto various (classical) water motions [Eq. (8)] are also shown: S_{trans} is the contribution of all c.m. translations, S_{long} is the projection onto the longitudinal component of the c.m. translations (see text), and S_{r-v} is the sum of the projections onto the vibrational and rotational motions. The normalization for all of the nonequilibrium curves is $\overline{\Delta E}(0) - \overline{\Delta E}(\infty) = 1.47$ eV. (b) The total equilibrium solvent response function [Eq. (7)] and integrated projections of it onto different classical motions [Eq. (9)]; the subscripts used for each projection are the same as in panel (a), except C_{r-v} also includes cross correlations. The error bars shown are ± 2 standard deviations [14]. The slight difference between the $C(t)$ curves in panels (a) and (b) results from a filter $\{\exp[-(t/1500 \text{ fs})^4]\}$ applied before integrating to obtain the curves in panel (b) [14].

lie between $\sim$1700 and $\sim$4000 cm^{-1}. We found (see EPAPS supplementary material [14]) that librations dominate both $S_{r\text{-}v}(t)$ and $C_{r\text{-}v}(t)$ and that vibrational coupling is negligible. Thus, the $S_{r\text{-}v}$ and $C_{r\text{-}v}$ curves plotted in Fig. 1 represent essentially pure librational projections of $S(t)$ and $C(t)$. Note that a spectral density analysis of the *total* $S(t)$ and $C(t)$ could not have distinguished contributions from translational or librational DOF since water translations and librations have overlapping frequency ranges. Our new formalism, however, allows us to cleanly isolate the role of each classical degree of freedom in the nonequilibrium solvent relaxation, $S(t)$, as well as all of the cross terms in the equilibrium solvent response, $C(t)$.

The projections of $S(t)$ and $C(t)$ make it easy to see that the classical motions underlying the equilibrium and nonequilibrium solvent relaxation of the e_{hyd}^{-} are quite different. Figure 1(b) shows that solvent librations and translations contribute equally to $C(t)$ [if we had examined only $G_{r\text{-}v}(t)$ and $G_{\text{trans}}(t)$, rather than integrating to obtain $C_{r\text{-}v}(t)$ and $C_{\text{trans}}(t)$, we would not know that rotations and translations couple with equal magnitude to $C(t)$ because the second derivatives contain information only about the curvature of the response, not the magnitude or time scales [14]]. In contrast, Fig. 1(a) indicates that librational motions, which move H atoms into the node of the excited *p*-like wave function [6], dominate the nonequilibrium solvent relaxation. Both at and away from equilibrium, translational solvent motions occur on a single time scale, with longitudinal motions comprising $\sim$90% of the total translational response. The librational responses, however, are quite different at and away from equilibrium. The equilibrium librational response, $C_{r\text{-}v}$, occurs on two distinct time scales and is characterized by a rapid inertial relaxation that accounts for $\sim$1/3 of the total solvation followed by a slower component that is not complete until $t > \sim$500 fs. In contrast, the nonequilibrium librational response, $S_{r\text{-}v}$, is nearly complete within $\sim$50 fs and plays only a minor role in the total nonequilibrium relaxation after 100 fs. Thus, our projection analysis demonstrates that not only do different solvent motions contribute to relaxation with different amplitudes at and away from equilibrium, but also that the equilibrium and nonequilibrium solvent dynamics are composed of entirely different types of solvent motions; the large size and shape changes that the e_{hyd}^{-} undergoes upon excitation alter the solute-solvent coupling, leading to a breakdown of LR [15].

In summary, we have presented a new formalism for projecting how classical motions affect quantum observables in MQC MD simulations. Our method can be applied to any quantum operator and provides precise, molecular detail about the coupling between quantum solutes and classical motions. We applied our method to study the solvent relaxation of the prototypical MQC system, the photoexcited e_{hyd}^{-}, and found that entirely different solvent motions were responsible for the equilibrium and nonequilibrium solvent relaxation, explaining the breakdown of LR for this system. Finally, our new formalism could be used to study how quantum-mechanical spins, electron or proton transfer reactions, and quantum-mechanical tunneling rates are modulated by specific bath DOF.

*Electronic address: schwartz@chem.ucla.edu
[1] W. A. Steele, Mol. Phys. **61**, 1031 (1987).
[2] B. M. Ladanyi and R. M. Stratt, J. Phys. Chem. A **102**, 1068 (1998).
[3] B. M. Ladanyi and M. Maroncelli, J. Chem. Phys. **109**, 3204 (1998).
[4] M. J. Bedard-Hearn, R. E. Larsen, and B. J. Schwartz, J. Phys. Chem. A **107**, 4773 (2003).
[5] M. J. Bedard-Hearn, R. E. Larsen, and B. J. Schwartz, J. Phys. Chem. B **107**, 14 464 (2003).
[6] B. J. Schwartz and P. J. Rossky, J. Chem. Phys. **101**, 6902 (1994).
[7] For the equilibrium solvation correlation function, $\Delta E = \langle 1|\hat{H}|1\rangle - \langle 0|\hat{H}|0\rangle$ is the energy gap between the ground ($|0\rangle$) and first excited ($|1\rangle$) states of the hydrated electron.
[8] R. E. Larsen, M. J. Bedard-Hearn, and B. J. Schwartz, J. Phys. Chem. (to be published).
[9] K. Toukan and A. Rahman, Phys. Rev. B **31**, 2643 (1985).
[10] P. J. Rossky and J. Schnitker, J. Phys. Chem. **92**, 4277 (1988).
[11] M. J. Bedard-Hearn, R. E. Larsen, and B. J. Schwartz, J. Chem. Phys. **123**, 234106 (2005).
[12] In MF-SD, the electronic density matrix undergoes discontinuities whenever the quantum subsystem decoheres (Ref. [11]). The resulting changes in the quantum energy are partitioned among the classical coordinates, and projections of these events onto the bath DOF are trivial (Ref. [13]). For a discussion of such rare events (which contribute negligibly to the nonequilibrium response) in our simulations, see EPAPS supplementary material [14].
[13] O. V. Prezhdo and P. J. Rossky, J. Chem. Phys. **107**, 825 (1997).
[14] See EPAPS Document No. E-PRLTAO-97-038639 for numerical details. For more information on EPAPS, see http://www.aip.org/pubservs/epaps.html.
[15] D. Aherne, V. Tran, and B. J. Schwartz, J. Phys. Chem. B **104**, 5382 (2000).
[16] If we had used only 20 trajectories (as in Ref. [6]) instead of 50, we would expect the error bars for $S(t)$ [Fig. 1(a)] to increase by $\sim$60%. This increased error could also cause $\overline{\Delta E}(\infty)$ to change by 20% to 30%. In combination, the increased error would make it easy to be convinced that $S(t) \sim C(t)$, as was concluded in Ref. [6].